2023 IEEE Conference on Control Technology and Applications (CCTA)
August 16-18, 2023. Bridgetown, Barbados

A Control-Oriented Modelica 1-D Model of a Planar Solid-Oxide Fuel Cell for Oxy-Combustion Cycles

Matteo Luigi De Pascali[1], Alessandro Donazzi[2], Emanuele Martelli[2] and Francesco Casella[1]

2023 IEEE Conference on Control Technology and Applications (CCTA) | 979-8-3503-3544-6/23/$31.00 ©2023 IEEE | DOI: 10.1109/CCTA54093.2023.10252534

***Abstract*— The authors propose an object-oriented Modelica 1-D SOFC model following the indications of a previous work. The model is intended to be used in the study of the SOS-CO_2 cycle for control studies purposes. The SOFC working conditions are challenging and require adapting the model to handle properly reformate mixtures at the anode and carbon dioxide-rich mixtures at the cathode while keeping its formulation as simple as possible. This paper reviews the previous contribution, adapts the model for the new working conditions, provides insights related to the Modelica implementation, reproduces the tests presented in literature and extends the validation through a comparison with experimental data. Finally the model is tested under SOS-CO_2 cycle operative conditions.**

I. INTRODUCTION

Carbon capture utilization and storage (CCUS) is a group of technologies recognized to play a key role for energy systems to meet international goals of emissions reduction [1]. Among CCUS technologies, oxy-combustion is a promising yet challenging technique exploiting combustion with pure oxygen to generate nitrogen-free flue gases. This allows, through water condensation, to obtain a carbon dioxide stream that can be later stored underground. Different system configurations featuring oxy-combustion have been investigated and the ones exploiting CO_2 in supercritical cycles are characterized by the highest efficiencies [2]. Recently, the innovative SOS-CO_2 cycle was proposed [3]; it can reach up to 75% efficiency while featuring a solid-oxide fuel cell (SOFC). In this plant, the SOFC is the main source of electrical power (about 70% of the gross power output) and works in unusual conditions: anodic and cathodic flows have high CO_2 molar fractions and the SOFC stack works at pressures as high as $40\,\mathrm{MPa}$. Moreover, the natural gas of the anodic inlet flow is not completely consumed in the fuel cell as happens in ordinary operations, but a small quantity is sent to the combustor that feeds the cycle's turbine.

This work is part of a project that aims at creating a Modelica [4] object-oriented model of the SOS-CO_2 cycle to study its dynamic behavior and possible ways of controlling it. For an in-depth discussion on why Modelica is worth employing for this kind of tasks, please refer to [5]. With this paper, the authors present a 1-D SOFC Modelica dynamic model capable of describing the relevant phenomena that regulate the fuel cell behavior and its temperature, composition and power profiles during operation. A multidimensional model would be unnecessarily complicated when included in the whole SOS-CO_2 plant. It is reasonable to assume that parallel channels work in a similar way and, for the purpose of system level studies, given the reduced dimensions of the solid parts in transverse direction, their description can be neglected resorting to a 1-D model. Moreover, a 0-D version would not capture correctly important dynamics phenomena related to thermal effects: since they influence SOFC durability and the temperatures at the inlet of the combustor and turbine, their evaluation is crucial while analyzing the plant during transient operations [6]. Mass accumulation effects are dominated by the inlet and outlet collectors at the fuel cell block boundaries and their design is not related to the one of the single SOFC module. However, both energy and mass balances are considered with the respective accumulation term to prevent the solver from computing solutions for big nonlinear algebraic systems of equations. Up to the authors' knowledge, only one paper has been published with a contribution related to object-oriented modeling of a SOFC [7]. With this work, it is intended to review the mentioned paper and extend its use case to SOS-CO_2 cycle, give insights regarding the Modelica implementation, reproduce the tests presented and extend the validation of the model through a comparison with experimental data. Finally the model is tested in the operating conditions of the SOS-CO_2 cycle.

II. MODELING

In this section the model of the SOFC is presented. While illustrating the physical equations, particular attention will be dedicated to the way they are implemented in Modelica language to ease their solution during model initialization and simulation. A SOFC model is composed by models describing the anodic and cathodic channels, the PEN (Positive-Electrolyte-Negative trilayer structure), the interconnecting plates, the working fluids, the chemical reactions and heat transfer phenomena. Figure 1 shows a schematic representation of a SOFC model. Finite discretization volumes are employed to model coupled anode and cathode channel sections separated by the respective membrane segment. These units are connected in series to obtain paired anodic and cathodic channels. Assuming that the parallel channels of a module work in similar conditions, SOFC modules are modeled just by multiplying the extensive variables of an assembled channel couple by the total number of channels.

The same assumptions made in [7] are considered. In particular, the most relevant are:

1) anodic and cathodic channel volumes are modeled as continuously stirred tank reactors;

[1]Politecnico di Milano, Dipartimento di Elettronica, Informazione e Bioingegneria, Italy (e-mail: matteoluigi.depascali@polimi.it, francesco.casella@polimi.it)

[2]Politecnico di Milano, Dipartimento di Energia, Italy (e-mail: alessandro.donazzi@polimi.it, emanuele.martelli@polimi.it)

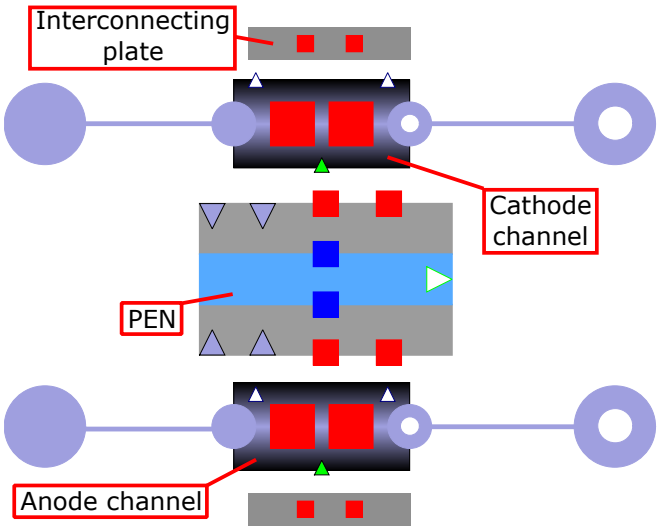

Fig. 1: Modelica model diagram for the fuel cell module.

2) hydrogen oxidation reaction (HOR) is modeled in the PEN; steam reforming (SR) and water gas shift (WGS) reactions are instantiated in the anodic channel model;
3) the temperature gradient across the PEN layers can be neglected;
4) heat conduction in the PEN along the flow direction is neglected as thermal power is considered to flow through contact with the running fluids.

A. Fluid model

Solid-oxide fuel cells can be supplied with different gas mixtures. While the reactions responsible for electric power production involve hydrogen and water, it is also possible to feed partially pre-reformed natural gas as an alternative to humidified hydrogen. Natural gas is converted in the anode to hydrogen through SR and WGS reactions. Thus, to model the thermodynamics of this reacting system it is requested to consider the enthalpies of reaction of the three reactions. They can be accounted evaluating the enthalpy of the mixtures considering as reference temperature $298\,\mathrm{K}$ and each species enthalpy of formation.
An ideal gas model is suitable to describe the mixture behavior up to considerable pressures (i.e. $10\,\mathrm{MPa}$) since the temperatures at which the SOFC operates are usually around $1000\,\mathrm{K}$. With Modelica, it is possible to exploit the Modelica.Media Library with the flag *excludeEnthalpyOfFormation* set to false or to implement a custom ideal gas model computing specific energy, specific enthalpy and specific volume and their derivatives with respect to temperature, pressure and composition.

B. Channel chemical reactions model

To model the kinetics of the phenomena occurring in the SOFC, HOR, SR and WGS reaction rates should be computed and included in mass and energy balances formulation. Since these reactions take place in the anode, the channel chemical reactions model will be instantiated just in the anode channel model. By previous assumptions, HOR is modeled in the PEN and its equations are not included in the chemical reaction model. Reaction rates as the ones reported in [7] should be substituted with the ones in equations (1) and (2) to model correctly the behaviour of the reactions in the SOS-CO_2 cycle configuration [8]. The simplified expressions do not allow to limit both SR and WGS to equilibrium conditions and lack partial pressures of every reactant.

$$r_{sr} = k_{0,sr} \cdot \exp\left(-\frac{E_{a,sr}}{RT}\right) p_{CH_4}\, p_{H_2O} \left(1 - \frac{k_{P,sr}}{k_{Eq,sr}}\right) \quad (1)$$

$$r_{wgs} = k_{0,wgs} \cdot \exp\left(-\frac{E_{a,wgs}}{RT}\right) p_{CO}\, p_{H2} \left(1 - \frac{k_{P,wgs}}{k_{Eq,wgs}}\right) \quad (2)$$

In the equations above E_a are the activation energies respectively assumed as $100\,\mathrm{kJ\,mol^{-1}}$ and $60\,\mathrm{kJ\,mol^{-1}}$ for SR and WGS [9] [10]; R is the universal gas constant, T the temperatures and p_i the partial pressures of the reactants. $k_{0,i}$ are the pre-exponential factors that can be tuned based on how fast reactions will reach their equilibrium. In both equations, k_P and k_{Eq} are equilibrium constants depending on components' activities and temperature respectively. Including them makes the reaction rate decrease as the reactions approach chemical equilibrium. Since $k_{Eq} = \exp\left(-\frac{\Delta g_0}{RT}\right)$, it is necessary to determine the Gibbs free energy variation (Δg_0 in $\mathrm{J\,mol^{-1}\,K^{-1}}$) with respect to standard conditions. Equations (3) and (4) are simplified expressions for SR and WGS reactions respectively [11].

$$\Delta g_{0,sr} = 4.1868 \cdot (53717 - 60.25 \cdot T) \quad (3)$$

$$\Delta g_{0,wgs} = 4.1868 \cdot (-8514 + 7.71 \cdot T) \quad (4)$$

Solving the initialization problem for this model can be numerically tricky, because the equations are strongly nonlinear and strongly coupled with each other. One way to improve the convergence of the initial solution is to use the homotopy operator (see [12] and [13] for more details) and initially set the temperature $T = T_{nom}$, thus decoupling chemical reactions from energy balances. The solution of the coupled equations is then obtained gradually via the homotopy transformation.

A final remark is due on equilibrium-limited kinetic models (1) and (2): if the pre-exponential factors are set excessively high, numerical solvers can produce noisy solutions, due to the very strong nonlinear behaviour; hence, a good compromise must be sought between having fast enough reactions, while avoiding numerical problems.

C. Channel model

Since anode and cathode channels contain different contributions in the mass and energy conservation equations, a partial model *BaseChannel* is created to group all the common variables and equations of the two models. Geometric parameters together with variables like inlet and outlet temperatures (T), enthalpies (h), pressures (p), mass flows (w) and mass fractions (X) are collected in this model. Heat transfer and working fluid models are instantiated

as *replaceable*: this allows to easily change them in case different modeling assumptions need to be considered.

BaseChannel includes also the inlet and outlet pneumatic ports for channel hydraulic series connection and two thermal ports to account for the convective heat transfer between the fluid and the solid parts (PEN and interconnecting plates).

A simplified linear momentum balance equation (5) may be implemented since the hypothesis of laminar flow is valid (see [14]). This formulation prevents the introduction of further nonlinearities linked to the pressure variable.

$$\Delta p = p_i - p_o = \frac{\Delta p_{nom}}{w_{nom}} \cdot w_i \tag{5}$$

Nominal values for mass flow and pressure drop are calibrated on design values.

Extending *BaseChannel*, it is possible to add the remaining equations to create the anodic and cathodic channel models. The following equations are the ones suited to describe the anodic side. For the cathodic channel, the terms related to the reaction rates are excluded while the terms related to O_2 transport have opposite signs.

Equation (6) is the standard mass balance accounting for $O^{=}$ ions migration from the cathode to the anode side. w_{O_2} is obtained with Faraday law as in equation (7). r_{hor} is HOR reaction rate and is shared from the PEN model through suitable input-output coupled connectors. i and o subscripts indicate inlet and outlet quantities.

$$\frac{\mathrm{d}M}{\mathrm{d}t} = w_i - w_o + w_{O_2} \tag{6}$$

$$w_{O_2} = \frac{r_{hor}}{2} \cdot \mathrm{MM}_{\mathrm{O_2}} \cdot S \tag{7}$$

$$\frac{\mathrm{d}M}{\mathrm{d}t} = -V\rho^2 \left(\frac{\partial v_o}{\partial T_o}\frac{\mathrm{d}T_o}{\mathrm{d}t} + \frac{\partial v_o}{\partial p_o}\frac{\mathrm{d}p_o}{\mathrm{d}t} + \frac{\partial v_o}{\partial \bar{X}_o}\frac{\mathrm{d}\bar{X}_o}{\mathrm{d}t} \right) \tag{8}$$

In equation (8) the time derivative of the total mass is expanded considering the derivatives of temperature, pressure and composition. Notice that the term $\frac{dM}{dt}$ in equations (6) and (8) is not expressed through the operator *der(M)*, but it is a variable to explicitly code a state change.

The conservation equations for the chemical species (9) are written with explicit derivatives of the mass fractions, coherently with the choice made for the overall mass balance. On the right-hand side, the stream terms are summed to the contributions of reactions and oxygen migration. $a_{j,r}$ are the stoichiometric coefficients describing the reactions and S is the contact surface between the fluid and the electrodes.

$$\begin{aligned} M\frac{\mathrm{d}X_{j,o}}{\mathrm{d}t} =& w_i \left(X_{j,i} - X_{j,o}\right) \\ &+ S \cdot \mathrm{MM}_j \sum_{r=1,3} a_{j,r} r_r - X_{j,o} w_{O_2} + w_{j,O2} \end{aligned} \tag{9}$$

Equation (10) is the energy balance for the anode channel. While Q_{plate} contribution is only provided by the convective thermal power transfer with the interconnecting plates, Q_{PEN} groups convection, oxygen migration and HOR heat of reaction extraction from the channel. This last term should be removed from the channel balance since species enthalpies include the formation term.

$$\begin{aligned} M\left(\frac{\partial u_o}{\partial T_o}\frac{\mathrm{d}T_o}{\mathrm{d}t} + \frac{\partial u_o}{\partial p_o}\frac{\mathrm{d}p_o}{\mathrm{d}t} + \frac{\partial u_o}{\partial \bar{X}_o}\frac{\mathrm{d}\bar{X}_o}{\mathrm{d}t} \right) =& w_i \cdot h_i \\ & - w_o \cdot h_o + Q_{PEN} + Q_{Plate} \end{aligned} \tag{10}$$

$$Q_{PEN} = Q_{ht,PEN} + w_{O_2} h_{O_2} + \Delta h_{0,hor} \cdot r_{hor} \cdot S \tag{11}$$

D. PEN model

The PEN model is the most critical component to implement since it describes extremely nonlinear electro-chemical phenomena. Adopting proper initialization strategies is of key importance to be able to simulate the model successfully. The model features four thermal power ports for convective exchanges with the fluid streams and radiative heat transfer with the interconnecting plates. Input and output ports are also present for signals measuring partial pressures in the channels and HOR reaction rate. Electrical pins from the Modelica Standard Library are employed to connect different SOFC modules on the electrical side. The electric potential difference between the pins is obtained through equation (12): losses related to activation overpotential (v_{act}), ohmic phenomena (v_{omh}) and diffusive resistance (v_{conc}) should be subtracted from the open circuit voltage V_{OCP}.

$$V_{PEN} = V_{OCP} - v_{ohm} - v_{conc} - v_{act} \tag{12}$$

Equation (13) shows how the open circuit voltage is evaluated. F is the Faraday constant, n is the number of electrons involved in the HOR (i.e. two), p_i are the partial pressures of products and reactants of HOR and p_{ref} is the reference pressure for species activities (101 325 Pa). Since $\Delta g_{0,hor}$ depends on temperature, integration of the Van't Hoff equation is requested to link these two quantities.

$$V_{OCP} = -\frac{\Delta g_{0,hor}}{nF} - \frac{RT}{nF} \cdot \ln\left(\frac{p_{H_2O}}{p_{H2} \cdot \sqrt{\frac{p_{O2}}{p_{ref}}}} \right) \tag{13}$$

To help reaching convergence during initialization, V_{PEN} and V_{OCP} expressions may be simplified with homotopy. The first quantity can be initially expressed through a linear approximation of a reference polarization curve. This allows to decouple the electro-chemical related equations of each module to ease their solution. Regarding the open circuit voltage, substituting the logarithmic term with an approximated constant value partially decouples mass fractions evaluation from the electro-chemical phenomena. If no reasonable value is available to describe the evolution of the partial pressures along the channel in the operative condition, an initialization with a non reacting mixture (e.g. humidified hydrogen) at low current allows to evaluate the simplified term. This can be obtained in two ways: the model can undergo a slow transient while the composition at the anodic entrance is gradually changed or homotopy can be used to include this process in the initialization.

Voltage losses formulation follows what is reported in [7] with exceptions for diffusion and activation contributions.

Instead of employing a fixed value for the diffusivity coefficient in the two electrodes, first-principles computation of $D^{eff}_{H_2O}$, $D^{eff}_{H_2}$ and $D^{eff}_{O_2}$ can be implemented. Based on the theory reported in [15], this approach allows to work with any fluid mixture fed to the cell. Furthermore, if the anode is porous enough, the concentration loss is almost linear with the current throughout the entire useful operating range. In this case, a simplified concentration loss model can be implemented through the evaluation of an equivalent resistance, employing the dusty gas model (as explained in reference [16]). However, if the porosity is not large enough, nonlinear behaviour can kick in, causing a sharp drop of voltage at high currents, similar to the one caused by high utilization factors [17].
Activation losses are evaluated through an implicit formula as reported in equation (14) and (15).

$$j = j_0^{el}\left[\exp\left(\frac{\beta nF}{RT_{PEN}}v_{act}^{el}\right) - \exp\left(-\frac{(1-\beta)\,nF}{RT_{PEN}}v_{act}^{el}\right)\right] \quad (14)$$

$$j_0^{el} = \frac{RT_{PEN}}{nF}k_{el}\cdot\exp\left(-\frac{E_{el}}{RT_{PEN}}\right) \quad (15)$$

It might be useful to make equation (14) explicit with respect to the activation losses as reported below

$$v_{act}^{el} = \frac{RT_{PEN}}{\beta nF}\ln\left(\frac{j}{2j_0^{el}} + \sqrt{\left(\frac{j}{2j_0^{el}}\right)^2 + 1}\right) \quad (16)$$

Equation (16) allows the use of the homotopy operator with the simplified expression $v_{act}^{el} = \frac{RT_{PEN}}{\beta nF}\frac{j}{j_0^{el}}$ to be used during initialization [18].

A correct estimation of k_{el} and E_{el} parameters is crucial for a successful modeling of the activation losses and of the overall polarization curve of the SOFC. These values have a wide range of variation as reported in [18]. We experienced convergence difficulties employing traditional gradient-based methods for identification, presumably because of the strong nonlinearities included in the model by Arrhenius-like equations. A particle swarm identification method [19] was instead successful.

E. Heat transfer model

The assumption of laminar flow in the channels simplifies Nusselt number evaluation. Values around Nu $= 4$ are assumed as suggested in [18]. The heat transfer coefficient α in equation (17) is evaluated through Nusselt number definition and employing empirical correlations for the thermal conductivity of the streams in the channels.

$$Q = S\cdot\alpha\cdot(T_{flow} - T_{wall}) \quad (17)$$

III. Results

The proposed model is first validated in the scenario shown in [7], reproducing the same results. Then, a polarization curve from [20] is taken as benchmark to show how the model can be tuned to fit experimental data. Finally the model is used to predict the behaviour in the SOS-CO_2 cycle conditions, for which no reference is known.

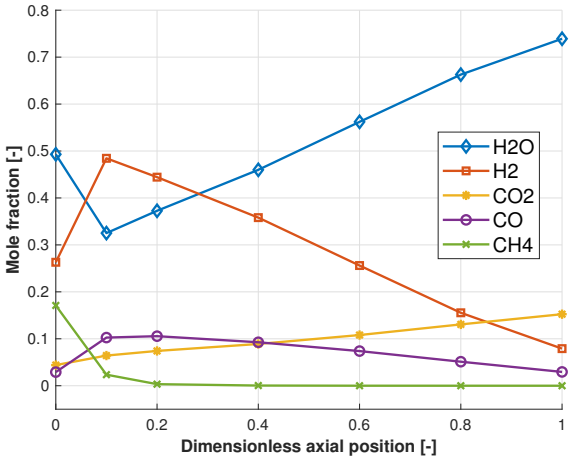

Fig. 2: Mole fraction evolution in the anodic channel.

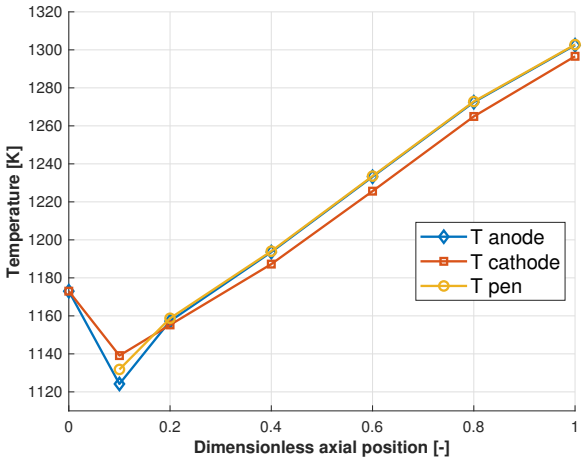

Fig. 3: Temperature distribution along the fuel cell

A. Comparison with simulated data

The first test takes as input the data from tables 3 and A.1 in [7] in the case of six discretization volumes. It should be noticed that the correct inlet molar fractions for the anode channel are 49.3% H_2O, 26.3% H_2, 4.4% CO_2, 2.9% CO and 17.1% CH_4. Note also that equation (34) from [7] is dimensionally wrong and should be replaced by the correct:

$$\lambda_{air} = 4F\frac{y_{O_2}w_{cat,in}}{i_{cell}MM_{air}} \quad (18)$$

with MM_{air} molar mass of air.

Figure 2 shows the evolution of the molar fractions of the species in the anodic channel at steady state. The results are coherent with the ones from [7]; the same can be said for the temperature profiles in figure 3. It should be pointed out that such temperature differences between the inlet and the outlet of a fuel cell are detrimental for the integrity of its solid parts and an higher mass flow rate at the cathodic channel should be employed to cool down the cell. Table I shows that voltage and extracted power match correctly.

TABLE I: Comparison between Ref. [7] and this work.

	Ref. [7]	This work
$V_{cell}\ [V]$	0.641	0.641
$P_{el}\ [W]$	19.3	19.3
Simulation time $[s]$	300	2

The simulation time has dramatically reduced thanks to the evolution of computer power and of Modelica tools. Unfortunately, explicit values for the cathodic activation energy E_{cat} and for the corresponding pre-exponential factor were not reported in the paper; hence, they were identified thanks to a particle swarm optimization routine. The obtained values are $E_{cat} = 139 \times 10^3\,\mathrm{J\,mol^{-1}}$ and $k_{cat} = 1 \times 10^{10}\,\mathrm{A\,m^{-2}}$, which are coherent with values found in literature.

B. Comparison with experimental data

To further extend the validation of the model, a polarization curve obtained in a lab experiment is reproduced taking as reference the conditions shown in figure 5 from [20]. It was not possible to compare the model with a real cell fed with partially reformed anodic stream since no polarization curve with such a boundary condition is present in literature. Although the supplied fuel is humidified hydrogen (6% H_2O, 94% H_2 molar basis), this scenario allows to formulate important observations to model fuel cell real behaviour.

To address this analysis, it should be noticed that lab experiments are much more difficult to replicate because of the high number of intrinsic uncertainties they carry. Figure 4 shows the comparison between the experimental polarization curve and the simulated one. In the experimental curve, the initial logarithmic decrease of the voltage caused by activation losses is absent and instead a linear trend is observed. At high current densities the voltage drops dramatically even though the fuel utilization factor is below 35%. These phenomena are caused by adverse lab experimental conditions: fuel leakages from the anodic to the cathodic side were noticed and the real amount of humidified hydrogen supplied was identified to be approximately one third of the reported data. Moreover, scanning electron microscope pictures showed a considerable decrease of the porosity of the cathode electrode in the proximity of the electrolyte membrane, which allows to explain the voltage drop by nonlinear effect of diffusion losses at high current density and low porosity. Current collection from the electrodes is also non ideal and difficult to represent through an equation based model like the one considered in this paper.

To model the low current density behaviour an additional loss is introduced as proposed in equation (19).

$$v_{leak} = v^0_{leak} \cdot \left(1 - \frac{i}{i_{max}}\right) \tag{19}$$

This term helps to decrease the ideal Nernst potential and lowers the first part of the polarization curve. v^0_{leak} and i_{max} are parameters that require appropriate tuning considering the

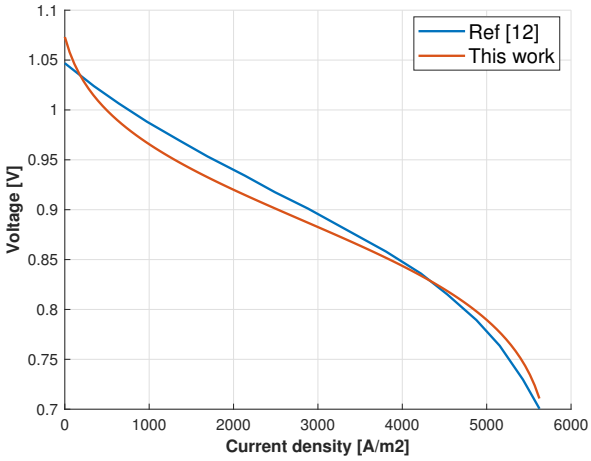

Fig. 4: Polarization curves: experimental data vs simulation.

entity of the loss. To fit the central and the final part of the curve, five parameters were considered as optimization variables in the identification problem: a generalized electrode activation energy and the respective pre-exponential factor, the porosity of the electrodes and the pre-exponential factors (γ_a and γ_{el}) of the anodic and electrolyte conductivities used to evaluate ohmic losses. Their values are reported in table II. The comparison between the two curves shows that the maximum errors committed is around 3% and is suitable with the purpose of the model, which is oriented towards control studies. However, it is worth noting that a properly engineered SOFC for the SOS-CO_2 cycle should not be affected by highly nonlinear diffusion losses, as it happened in these experimental results.

C. SOS-CO_2 scenario

The conditions in which the fuel cell operates in the SOS-CO_2 cycle are even more peculiar than just feeding partially pre-reformed fuel to the anodic channels and no data are available to the authors to validate the fuel cell model under these circumstances. Hence, in the following studies about the SOS-CO_2 cycle, model equations will be trusted in the light of the validations presented in the previous sections. Although the conditions reported in section III-B are relevant for laboratory experiments, we expect cells to work in more suited working ranges. Thus, the following results are obtained considering an higher utilization factor and the appropriate kinetic expressions ((1) and (2)).

TABLE II: Parameters resulting from identification routine to reproduce polarization curve from Ref. [20].

$E_{elec}\ [\mathrm{J\,mol^{-1}}]$	90e3
$k_{elec}\ [\mathrm{A\,m^{-2}}]$	1e12
$porosity\ [-]$	0.069
$\gamma_a\ [\Omega^{-1}\,\mathrm{m^{-1}}]$	3.32e6
$\gamma_{el}\ [\Omega^{-1}\,\mathrm{m^{-1}}]$	7.9e3

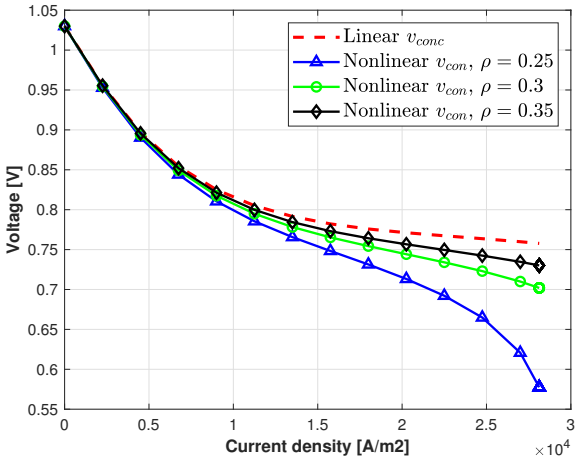

Fig. 5: SOS-CO_2 polarization curves: linear vs nonlinear concentration losses at different electrode porosity ρ.

Table III lists the boundary conditions with which the SOFC was tested. To employ the ideal gas model, the considered pressure p is lowered to a less challenging operating condition as reported in [3]. In case of higher values, a model describing real gas effects can be easily replaced thanks to the flexibility offered by the Modelica language. Figure 5 shows polarization curves obtained with the previously specified conditions: the high operative pressure helps keeping open circuit voltage above 1 V despite the unfavorable composition of the working fluids. Changing electrodes' porosity greatly influences the output voltage of the cell when considering the nonlinear concentration losses model, especially at higher current densities. The linear model is sufficiently accurate when the porosity is high enough or when lower current densities are extracted.

IV. Conclusion

An object-oriented Modelica 1-D SOFC model has been developed with the purpose of integrating it in the SOS-CO_2 cycle model. While reviewing and adapting an existing model, the authors have highlighted the crucial aspects to consider to extend the validity of the presented SOFC model. Important insights were also given regarding the Modelica implementation. The model has been tested successfully in different case scenarios, including the comparison with both simulations and experimental data. Since no references are available, the results, related to the peculiar conditions in which the SOFC of the SOS-CO_2 cycle works, are the first of their kind and offer a starting point for further developments. The Modelica code of the SOFC is available here [21].

TABLE III: Boundary conditions for SOS-CO_2 cycle conditions.

I_{max} [A]	45
U_f [–]	0.7
$T_{in,anode}$ [K]	930
$T_{in,cathode}$ [K]	783
p [MPa]	2.75
Composition	Table 1, FU3 and FU4, Ref. [3]
Cell area $[m^2]$	1.6e-3

Acknowledgment

This work is supported by the Italian Ministry of University and Research under the PONRI program (Programma Operativo Nazionale "Ricerca e Innovazione" 2014-2020).

References

[1] IEA, "CCUS in clean energy transitions," 2020. [Online]. Available: https://www.iea.org/reports/ ccus-in-clean -energy-transitions

[2] R. Scaccabarozzi, M. Gatti, and E. Martelli, "Thermodynamic analysis and numerical optimization of the NET Power oxy-combustion cycle," *Applied energy*, vol. 178, pp. 505–526, 2016.

[3] R. Scaccabarozzi *et al.*, "Solid oxide semi-closed CO2 cycle: A hybrid power cycle with 75% net efficiency and zero emissions," *Applied Energy*, vol. 290, p. 116711, 2021.

[4] S. E. Mattsson *et al.*, "Physical system modeling with Modelica," *Control Engineering Practice*, vol. 6, no. 4, pp. 501–510, 1998.

[5] F. Casella and A. Leva, "Modelling of thermo-hydraulic power generation processes using Modelica," *Mathematical and Computer Modelling of Dynamical Systems*, vol. 12, no. 1, pp. 19–33, 2006.

[6] C.-K. Lin *et al.*, "Thermal stress analysis of a planar SOFC stack," *Journal of Power Sources*, vol. 164, no. 1, pp. 238–251, 2007.

[7] A. Salogni and P. Colonna, "Modeling of solid oxide fuel cells for dynamic simulations of integrated systems," *Applied Thermal Engineering*, vol. 30, no. 5, pp. 464–477, 2010.

[8] K. Ahmed and K. Foger, "Analysis of equilibrium and kinetic models of internal reforming on solid oxide fuel cell anodes: Effect on voltage, current and temperature distribution," *Journal of Power Sources*, vol. 343, pp. 83–93, 2017.

[9] V. N. Nguyen *et al.*, "Methane/steam global reforming kinetics over the Ni/YSZ of planar pre-reformers for SOFC systems," *Chemical Engineering Journal*, vol. 292, pp. 113–122, 2016.

[10] J. Xu and G. F. Froment, "Methane steam reforming, methanation and water-gas shift: I. intrinsic kinetics," *AIChE journal*, vol. 35, no. 1, pp. 88–96, 1989.

[11] G. Natta and I. Pasquon, *Prinicipi della chimica industriale. Applicazioni della termodinamica alle reazioni della grande chimica industriale*. Tamburini Editore, 1993, p. 91.

[12] F. Casella *et al.*, "Steady-state initialization of object-oriented thermo-fluid models by homotopy methods," in *Proceedings of the 8th International Modelica Conference; March 20th-22nd; Technical Univeristy; Dresden; Germany*, no. 063. Linköping University Electronic Press, 2011, pp. 86–96.

[13] M. Sielemann *et al.*, "Robust initialization of differential-algebraic equations using homotopy," in *Proceedings of the 8th International Modelica Conference; March 20th-22nd; Technical Univeristy; Dresden; Germany*, no. 063. Linköping University Electronic Press, 2011, pp. 75–85.

[14] A. Donazzi *et al.*, "A quasi 2D model for the interpretation of impedance and polarization of a planar solid oxide fuel cell with interconnects," *Electrochimica Acta*, vol. 365, p. 137346, 2021.

[15] E. L. Cussler, *Diffusion: mass transfer in fluid systems*. Cambridge university press, 2009, pp. 119–122.

[16] Y. Fu *et al.*, "Multicomponent gas diffusion in porous electrodes," *Journal of The Electrochemical Society*, vol. 162, no. 6, p. F613, 2015.

[17] M. Ni, M. K. Leung, and D. Y. Leung, "Parametric study of solid oxide fuel cell performance," *Energy Conversion and Management*, vol. 48, no. 5, pp. 1525–1535, 2007.

[18] S. Campanari and P. Iora, "Definition and sensitivity analysis of a finite volume SOFC model for a tubular cell geometry," *Journal of Power Sources*, vol. 132, no. 1-2, pp. 113–126, 2004.

[19] N. Hansen and A. Ostermeier, "Completely derandomized self-adaptation in evolution strategies," *Evolutionary computation*, vol. 9, no. 2, pp. 159–195, 2001.

[20] A. Cammarata *et al.*, "Numerical and experimental assessment of a novel SOFC-based system for micro-power generation," *Journal of Power Sources*, vol. 551, p. 232180, 2022.

[21] M. De Pascali and F. Casella, "SOFCPoliMi library," https://github.com/looms-polimi/SOFCPoliMi, 2023.